Room Temperature Phosphorescence in Solution from Thiophene-Bridged Triply Donor-Substituted Tristriazolotriazines

Hugo Marchi Luciano, Giliandro Farias, Cristian Salla, Larissa Franca, Suman Kuila, Andrew Monkman, Fabien Durola, Ivan Bechtold, Harald Bock, Hugo Gallardo

Room Temperature Phosphorescence in Solution from Thiophene-Bridged Triply Donor-Substituted Tristriazolotriazines

Hugo Marchi Luciano,[a, b] Giliandro Farias,[a] Cristian M. Salla,[c] Larissa G. Franca,[d] Suman Kuila,[d] Andrew P. Monkman,[d] Fabien Durola,[e] Ivan H. Bechtold,*[c] Harald Bock,*[e] and Hugo Gallardo*[a]

Abstract: Most organic room-temperature phosphorescence (RTP) emitters do not show their RTP in solution. Here, we incorporated sulfur-containing thiophene bridges between the donor and acceptor moieties in D_3A-type tristriazolotriazines (TTTs). The thiophene inclusion increased the spin-orbit coupling associated with the radiative $T_1 \rightarrow S_0$ pathway, allowing RTP to be observed in solution for all compounds, likely assisted by protection of the emissive TTT-thiophene core from the environment by the bulky peripheral donors.

Introduction

Room-temperature phosphorescence (RTP) from non-metalated organic chromophores offer a fascinating alternative to organometallic complexes, and has been widely used in electroluminescence and bio-imaging technologies.[1] Organometallic RTP complexes often include heavy transition metals like Ir or Pt that induce strong spin-orbit coupling (SOC) and alleviate two 'spin-forbidden' processes, that is, intersystem crossing (ISC) between the S_1 and T_1 states and the following radiative $T_1 \rightarrow S_0$ transition.[2] Metal-free organic chromophores require specific functional groups, most notably aromatic carbonyls, in order to generate triplet excitons through El-Sayed-allowed π–π^* and n–π^* transitions between the singlet and triplets.[3] These materials have long been used as photosensitizers. However, phosphorescence in fluid solution is often quenched by rapid non-radiative deexcitation of the chromophores by solvent collisions and rotational motions. Therefore, they require a dense, highly ordered crystalline network, or a rigid glassy polymer matrix to suppress molecular motions.[4] Although a few molecular systems have been shown to generate solution state RTP when encapsulated in supramolecular hosts, matrix-free systems are extremely rare.[5] Therefore, new design principles for enhanced ISC and subsequent RTP are essential to provide organic phosphors that function in a matrix-free liquid environment. Such materials are potentially more useful for bioimaging with lesser interference from the solvent medium. Herein, we designed a series of donor-acceptor molecules with a rigid acceptor core (to minimise vibrational dissipation) and we anticipated that a multiple donor substitution would contribute to protect the triplet-emitting core from de-excitating solvent interactions. Donor-acceptor molecules have long been studied for thermally activated delayed fluorescence (TADF) owing to their small ^{1}CT-^{3}CT energy gaps (CT = charge transfer state). Ethertington et al. have shown that a secondary ^{3}LE state mediates the ISC process between these CT manifolds for stronger spin-orbit coupling.[6] These ^{3}LE states can have significant SOC with the ^{1}CT according to El-Sayed's rule.

D_3A structures where the electron acceptor TTT is surrounded by three donor substituents have recently been shown to be interesting candidates for efficient blue emission either via the TADF mechanism, or via similar triplet-to-singlet intersystem crossing (ISC) from Kasha-forbidden higher triplet states.[7]

ISC relies on efficient SOC, and SOC increases dramatically with increasing weight of the atoms on which the relevant orbitals are located. The incorporation of sulfur atoms has accordingly been shown to improve significantly the efficiency of TADF-based organic light emitting diodes (OLEDs).[8]

[a] *H. Marchi Luciano, Dr. G. Farias, Prof. H. Gallardo*
Departamento de Química
Universidade Federal de Santa Catarina
Trindade, 88040-900 Florianópolis, SC (Brazil)
E-mail: hugo.gallardo@ufsc.br

[b] *H. Marchi Luciano*
Centre de Recherche Paul Pascal
Université Bordeaux
115 av. Schweitzer, 33600 Pessac (France)

[c] *Dr. C. M. Salla, Prof. I. H. Bechtold*
Departamento de Física
Universidade Federal de Santa Catarina
Trindade, 88040-900 Florianópolis, SC (Brazil)
E-mail: ivan.bechtold@ufsc.br

[d] *L. G. Franca, Dr. S. Kuila, Prof. A. P. Monkman*
Department of Physics
Durham University
Durham DH1 3LE (UK)

[e] *Dr. F. Durola, Dr. H. Bock*
Centre de Recherche Paul Pascal, CNRS
115 av. Schweitzer, 33600 Pessac (France)
E-mail: harald.bock@crpp.cnrs.fr

We have now incorporated sulfur-containing thiophene bridges in the place of the usual phenylene spacers between the donor and acceptor moieties in D_3A-type TTTs to probe the effect of the sulfur heavy atom on the emission behavior. To limit the conjugation between the donor and acceptor moieties and thus minimize both LUMO-HOMO overlap and the energy gap ΔE_{ST} between the S_1 and T_1 states, we chose a 2,4 substitution pattern on the thiophene bridges instead of the more common 2,5 pattern. Such 2,4-disubstitution on thiophene is analogous to 1,3-disubstitution on benzene, whereas 2,5-disubstitution is analogous to 1,4-disubstitution on benzene, and it has been shown that meta-disubstitution on benzene linkers leads to smaller ΔE_{ST} and increases delayed emission by several orders of magnitude in tricarbazolyl-triphenyltriazine.[9] Thus we prepared four 2,4-thiophene-bridged target compounds **1a–d** where the thiophene bridge is linked in position 2 to the TTT core and in position 4 either to di-3,6-tert-butyl-carbazole (in **1a** & **1b**) as weaker donor or 9,9-dimethyl-9,10-dihydroacridine (DMAc, in **1c** & **1d**) as stronger donor, using either plain thiophene (in **1a** & **1c**) as bridge or 5-methyl-substituted thiophene (in **1b** & **1d**) to increase the torsion angle with the donor.

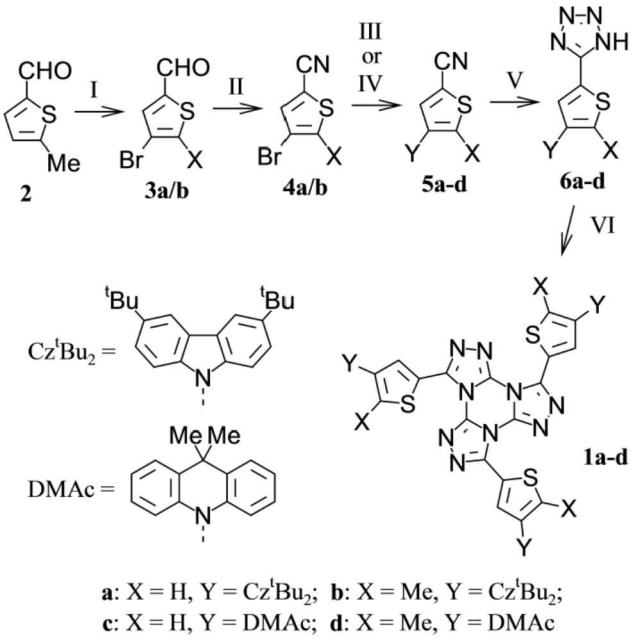

Scheme 1. I) Br_2, AcOH, **3b**: 60%; II) NH_4OH(aq), I_2, THF, **4a**: 82%, **4b**: 72%; III) 3,6-di-tert-butyl-9H-carbazole, K_2CO_3, $CuSO_4.5H_2O$, 1-methylnaphthalene, **5a**: 48%, **5b**: 34%; IV) 9,9-dimethyl-9,10-dihydroacridine, [$Pd(OAc)_2$], Xphos, NaOt–Bu, toluene, **5c**: 42%, **5d**: 46%; V) NaN_3, NH_4Cl, DMF, **6a**: 88%, **6b**: 83%, **6c**: 81%, **6d**: 79%; VI) $C_3N_3Cl_3$, 2,6-lutidine, toluene, **1a**: 38%, **1b**: 32%, **1c**: 39%, **1d**: 35%.

Results and Discussion

The most suitable method for synthesizing the TTT heterocycle is Huisgen's method, that is, the acylation of tetrazole with cyanuric chloride followed by triple thermal nitrogen elimination and ring closure. This method allows the obtention of various substituted TTTs, such as **1a–d** investigated here, from tetrazole derivatives. Thus, the design of different 5-substituted tetrazoles (**6a–d**) is the approach used here (Scheme 1). All required tetrazoles are synthesized from the corresponding aldehyde. **3a** was acquired commercially, but aldehyde **3b** was prepared by bromination of commercial reagent **2**. The aldehyde group of intermediates **3a/b** is converted to a cyano group (**4a**: 82% and **4b**: 72%) by oxidation with iodine and ammonium hydroxide. Two different C–N coupling strategies were used depending on the donor species. 3,6-di-tert-butyl-9H-carbazole reacts with the intermediate **4a/b** via a variant of the Ullmann condensation to yield the intermediates **5** (**5a**: 48%, **5b**: 34%). Compounds **5c** and **5d** (**5c**: 42% and **5d**: 46%) are obtained by palladium-catalyzed C–N coupling between intermediate **4a/b** and 9,9-dimethyl-9,10-dihydroacridine. In the next step, the cyano group of **5a–d** is converted to the tetrazole heterocycle (**6a–d**, ca. 80%) via a 1,3-dipolar cycloaddition with sodium azide. The target TTTs **1a–d** (~35%) were obtained by threefold reaction of cyanuric chloride with the 5-substituted tetrazoles (**6a–d**).

TGA analyses were carried out to study the emitters' thermal stability in N_2 with heating rate of 10 °C min^{-1} (Figure S1 in Supporting Information). All four donor-functionalized tristriazolotriazine compounds showed a decomposition temperature (defined as 3% of mass loss) in the range of 400–450 °C. **1c** (T_{dec} = 401 °C) and **1d** (T_{dec} = 402 °C) showed to be less thermally stable than the analogues containing the 3,6-di-tert-butyl-9H-carbazole unit, **1a** (T_{dec} = 442 °C) and **1b** (T_{dec} = 449 °C). The thermal stability of all four compounds under inert conditions is thus largely satisfactory for practical applications.

The redox properties of the TTT emitters were investigated by cyclic voltammetry (CV) measurements in DMF solution. As shown in Figure 1, for the emitters **1a** and **1b**, irreversible oxidation (E_{ox}) signals were detected in the range of ~1.5–1.6 V. Emitters **1c** and **1d** show quasi-reversible oxidation in the range of ~1.2–1.3 V. According to the oxidation onset, the E_{ox}

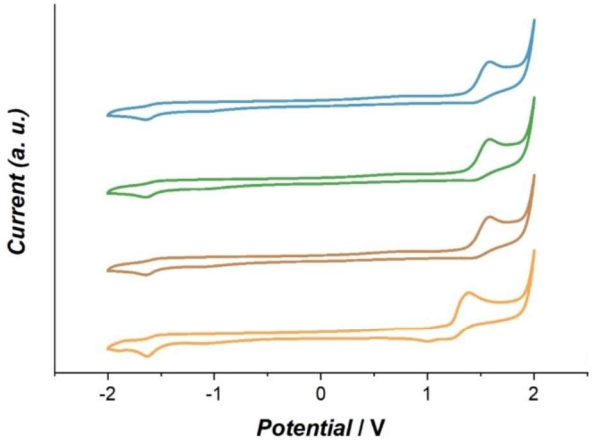

Figure 1. CV curves of the TTT emitters in DMF solution. 0.1 mol L^{-1} of Bu4NPF6 (tetrabutylammonium hexafluorophosphate) as a supporting electrolyte; scan rate: 100 mV s^{-1}; blue = **1a**, green = **1b**, brown = **1c**, orange = **1d**.

are 0.88 V for **1a**, 0.94 V for **1b**, 0.58 V for **1c** and 0.60 V for **1d** relative to ferrocenium/ferrocene (Fc/Fc^+, $E_{Fc/Fc+} = 0.46$ V). The smaller oxidation potential values observed in compounds with the 9,9-dimethyl-9,10-dihydroacridine moiety underline their stronger donor character relative to the 3,6-di-tert-butyl-carbazole moiety. Due to the common acceptor unit, similar reduction potential values were found: −2.30, −2.40, −2.29 and −2.34 V for **1a**, **1b**, **1c** and **1d** respectively. According to the formulas $E_{HOMO} = -(E_{ox}-E_{Fc/Fc+} + 4.8)$ eV and $E_{LUMO} = -(E_{red}-E_{Fc/Fc+} + 4.8)$ eV, the HOMO/LUMO energy levels of the emitters were calculated as −5.68/−2.50 eV (**1a**), −5.74/−2.40 eV (**1b**), −5.38/−2.51 eV (**1c**) and −5.40/−2.46 eV (**1d**). Correspondingly, the energy gaps are evaluated as 3.18, 3.34, 2.87, and 2.94 eV for **1a**, **1b**, **1c**, and **1d**, respectively.

These band gaps, larger for the carbazole derivatives **1a**&**1b** than for the acridine derivatives **1c**&**1d**, and larger for methyl-bearing **1b**&**1d** than for methyl-free **1a**&**1c**, are coherent with the weaker donor strength in **1a**&**1b** and the reduced spatial HOMO-LUMO overlap in **1b**&**1d**.

With all compounds **1a–d**, a high energy absorption band (at ca. 280 nm) is observed in toluene solution (Figure 2) and assigned to the π-π* transition of the TTT core.[5] For **1a** and **1b**, an absorption band close to 340 nm can be ascribed to the carbazole π-π* transition. For **1c** and **1d**, the corresponding band, at 320 nm, is assigned to the π-π* transition of the acridine moiety. Besides these bands characteristic for the individual subunits, broad and weak ($< 1000\ mol^{-1}\,L\,cm^{-1}$) absorption bands are observed at longer wavelengths which are associated to an intramolecular charge transfer (CT) state. In the acridine derivatives **1c** and **1d**, this band is weaker than in the carbazole derivatives **1a** and **1b**. This suggests that the acridine donor and TTT acceptor units are nearly orthogonal, forming a CT state with small oscillator strength (*f*).

The steady-state photoluminescence spectra (Figure 2) of the carbazole derivatives **1a** and **1b** show a slightly structured emission peak in dilute toluene solution, with maxima at 440 nm and 430 nm, respectively. As discussed below, this emission comes from a mixed ^{1}LE/^{1}CT state (^{1}LE = locally excited singlet, ^{1}CT = charge transfer singlet). Surprisingly, with the acridine derivatives **1c** and **1d**, when excited at around 320 nm, we can observe a dual emission. While the higher energy peak (ca. 350 nm) matches with the acridine moiety emission as previously reported by Rama et al.,[10] the second broad emission peak at around 460 nm is assigned to a ^{1}CT emission. The observed emission from the acridine moiety demonstrates the strongly decoupled nature of the donor and acceptor moieties in these molecules.

By increasing solvent polarity, a slight red-shift of the emission is observed for the carbazole derivatives, and the peak becomes less structured, confirming the mixed ^{1}LE/^{1}CT state (Figure S2a,b). In the higher-polarity solvent 2-MeTHF, **1c** (Figure S2c) shows a broader emission band, which could be related to the CT state stabilization and increased phosphorescence contribution to the overall emission. The emission is red-shifted for **1d** (Figure S2d), and the broadening in 2-MeTHF is much stronger. The higher phosphorescence contribution was confirmed by time-resolved photoluminescence (TRPL) described below.

To investigate the dynamics of the excited states, we performed TRPL measurements in toluene, and the decay curves are shown in Figure 3. The TRPL spectra show similar features in both carbazole derivatives (Figure S3a,b). In the first few nanoseconds, **1a** and **1b** show an emission peak centered at 440 nm and 415 nm, respectively. This peak is related to the

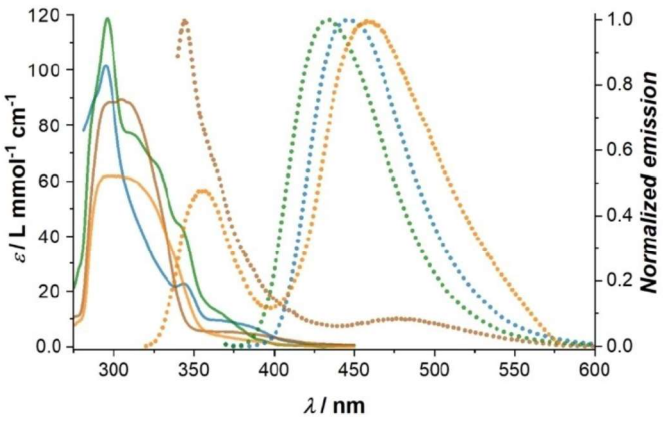

Figure 2. Absorption and emission spectra of **1a–d** in dilute toluene solution (10^{-5} mol L^{-1}); blue = **1a**, green = **1b**, brown = **1c**, orange = **1d**.

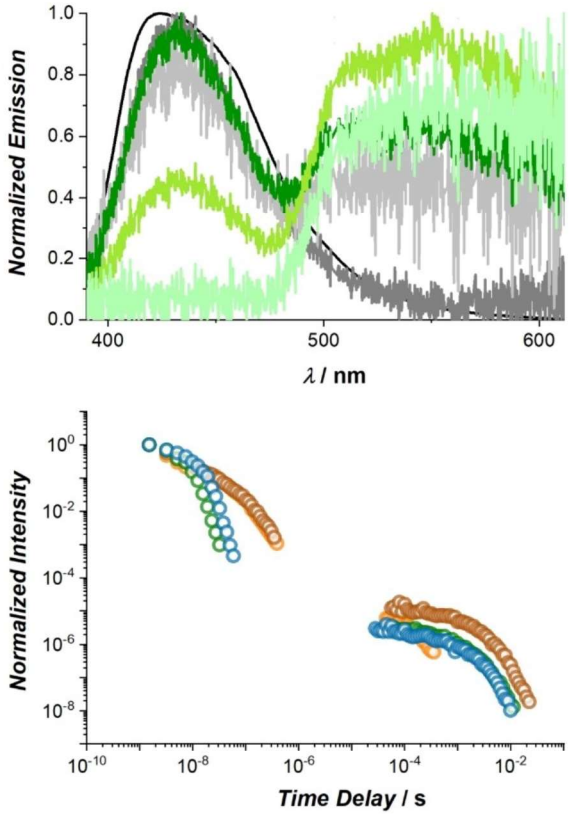

Figure 3. Top: Normalized spectra of **1b** in toluene solution taken at room temperature after different delay times; black = 1.5 ns, gray = 23 ns, light gray 0.11 ms, dark green = 0.50 ms, green = 2.5 ms, light green = 7.0 ms. Bottom: Time-resolved decay curves of **1a-d** in toluene; blue = **1a**, green = **1b**, brown = **1c**, orange = **1d**. The excitation wavelength was 355 nm. All measurements were performed in the absence of oxygen.

^{1}LE/^{1}CT state decaying with a lifetime of 7.3 ns for **1a** and 4.3 ns for **1b**. By increasing the delay times, we observed a regime of dual emission in the two carbazole derivatives. The short-wavelength band in the microsecond time regime has identical spectra as the prompt decay and is ascribed to delayed fluorescence (DF). The DF mechanism is likely related to triplet-triplet annihilation (TTA) because of the large ΔE_{ST} gap (Table 1) found for all four molecules. On the other hand, the second band, with onset at 575 nm for both compounds, displays characteristics typical of room-temperature phosphorescence (RTP), which, according to our theoretical investigations, arises from the TTT-thiophene core (^{3}LE). From the TRPL spectra, we observed that the DF emission decays faster, with lifetimes of 0.5 ms and 0.7 ms for **1a** and **1b**. The phosphorescence lifetime is around 3 ms for both compounds.

Moving from the carbazole derivatives to the acridine homologs, the TRPL spectra of **1c** in toluene solution show a similar trend (Figures S3c,d). Initially, **1c** undergoes a very rapid stabilization of the ^{1}CT state within a 2.3 ns lifetime, which then, with a broad emission band at around 460 nm decays within a 30.2 ns lifetime. At longer time delay, the dual emission related to TTA and RTP is observed with lifetimes of 0.8 ms and 3.5 ms. For **1d**, we only observed distinct differences at later times. This molecule, contrary to the other homologs, showed no detectable TTA and only a weak RTP with a short lifetime of 0.1 ms. The RTP in toluene solution displayed by all four compounds is somewhat unexpected. Evident RTP in solution is not usual, as triplet states have a long lifetime and usually undergo non-radiative decays. In our case, the bulky donor groups surrounding the rigid core most probably protect the ^{3}LE centered at the TTT-thiophene core from non-radiative losses (collisional deactivation with the environment). An exception is **1d**, where the larger SOC between the low-lying states and a higher triplet energy enhances the phosphorescence rate, as further discussed in the theoretical section.

To understand the role of the non-radiative rates in these molecules, we measured the absolute photoluminescence quantum yield (PLQY) in toluene solution (Table 1). We performed the PLQY measurements under air and calculated the PLQY in degassed solution ($\Phi_{degassed}$) from the PL ratio between degassed and air-equilibrated solution (Figure S4). The slight decrease of PL by introducing oxygen into the solution is mainly attributed to the quenching of the TTA mechanism. Oxygen quenches slow emissive processes, such as TTA and RTP, which involve triplet excited states. In toluene solution, the acridine derivatives presented significantly lower PLQY values than the carbazole derivatives. This corroborates with the acridine unit being more orthogonally positioned (close to 90°) to the core than the carbazole unit. Thus, even though it forms a CT state, this state has a small oscillator strength and, consequently, a lower radiative rate. The PLQY results indicate that all molecules present relatively strong spin-orbit coupling between the low-lying states due to the thiophene moiety, yielding a large population of triplet states ($\Phi_{ISC} = 1-\Phi_{degassed}$) and triplet non-radiative deactivation, especially on the acridine derivatives.

Solid-state photophysical properties of the emitters were measured in zeonex matrix, a non-polar saturated hydrocarbon polymer. Figure S5 shows the absorption and emission spectra for all four compounds. The two carbazole derivatives showed a similar absorption profile in zeonex as in toluene. In contrast, the acridine derivatives show better-resolved vibronic peaks in zeonex, consistent with the more rigid structure in the matrix. The photoluminescence of all compounds has a Gaussian-shaped emission band with similar onset as observed in toluene solutions, except for **1d**, probably due to a significantly broader distribution of donor-acceptor dihedral angles locked in the solid matrix. Figure S6 shows TRPL decay curves for all compounds. The decay curves show two regimes, a prompt regime followed by phosphorescence emission. For all compounds, a lifetime of around 3 ns is observed in the prompt regime at room temperature (Table 2). In zeonex, the TRPL decays from the two acridine homologs are more structured. The bulky matrix probably flattens the acridine compounds leading to mixed ^{1}LE/^{1}CT states as already observed with the carbazole derivatives in toluene, and thus, for all compounds, similar lifetimes are obtained in zeonex. In the slow regime, ^{3}LE emission from the TTT-thiophene core is observed with a lifetime of a few ms for all compounds. The slight increase in the lifetime is attributed to the decrease of the non-radiative

Table 1. Lifetimes τ and quantum yields Φ in toluene solution.

	1a	1b	1c	1d
τ_1 [ns]	–	–	2.3 (84%)	1.5 (89%)
τ_2 [ns]	7.3	4.3	30.2 (16%)	32.7 (11%)
τ_{DF} [ms]	0.5 (75%)	0.7 (83%)	0.8 (67%)	–
τ_{Phosph} [ms]	2.8 (25%)	3.2 (17%)	3.5 (33%)	0.1
Φ_{air} [a]	0.258	0.196	0.017	0.023
$\Phi_{degassed}$ [a]	0.304	0.232	0.023	0.029

[a] The error of Φ was ±0.01.

Table 2. Lifetimes τ, quantum yields Φ and S_1&T_1 energies in zeonex matrix.

	1a	1b	1c	1d
Room temperature:				
τ_{PF} [ns]	3.9	2.6	3.8	3.4
$\tau_{Phosph\ 1}$ [ms]	4.7	8.3	1.2 (82%)	0.8 (68%)
$\tau_{Phosph\ 2}$ [ms]	–	–	12.7 (18%)	7.3 (32%)
$\tau_{Phosph\ av}$ [ms] [b]	–	–	9.3	6.1
Φ_{air} [a]	0.144	0.124	0.031	0.055
80 K:				
τ_{PF} [ns]	7.7	6.0	5.1	4.7
$\tau_{Phosph\ 1}$ [ms]	20.4	20.7	0.9 (59%)	0.6 (51%)
$\tau_{Phosph\ 2}$ [ms]	–	–	16 (48%)	21 (49%)
$\tau_{Phosph\ av}$ [ms] [b]	–	–	14.6	20.5
S_1 [eV]	3.121 ± 0.020	3.229 ± 0.017	2.983 ± 0.015	3.103 ± 0.016
T_1 [eV]	2.475 ± 0.015	2.520 ± 0.010	2.480 ± 0.010	2.524 ± 0.008
ΔE_{ST} [eV]	0.646	0.709	0.503	0.579

[a] The error of Φ was ±0.01. [b] Obtained from $\tau = \Sigma\, \tau_i^2 A_i / \Sigma \tau_i A_i$, due to multi-exponential profile.

decay at the solid state. Furthermore, the similar lifetimes of solution and solid-state corroborate with the bulky donor moiety protecting the emissive core from the environment and allowing the RTP.

On decreasing the temperature, the spectra become better resolved in the prompt and the phosphorescence regime, indicating less motion and a more rigid structure in the film. Moreover, all compounds present similar lifetimes at low temperatures, whereas the non-radiative decays are less pronounced. From the onset values of the ^{1}LE/^{1}CT emission peak at room temperature and of the ^{3}LE emission peak at low temperature, we obtain a large ΔE_{ST} gap of more than 0.5 eV for all molecules. Such large ΔE_{ST} gaps rule out the TADF mechanism at room temperature. The ^{3}LE energy values are similar for all compounds, implying a minimal influence of the modifications on the TTT core.

DFT calculations were performed to obtain the ground state geometries, and for all compounds, the bonds and angles are in good agreement with similar compounds where X-ray structures were obtained.[11] The orthogonality of the donor-acceptor moieties was evaluated by measuring the dihedral angles between the TTT core and the thiophene moiety, and between the thiophene moiety and the donor unit (carbazole or acridine). For **1a** and **1b**, the average TTT-thiophene angles of 15.76° and 13.20° illustrate that these units are not coplanar. The thiophene-carbazole angle increases from 41.43° in **1a** to 61.08° in **1b**. As the TTT-thiophene dihedral angles are similar for both compounds, the thiophene-carbazole angle determines that the carbazole moiety is more orthogonal to the TTT core in **1b**. For **1c** and **1d**, similar TTT-thiophene dihedral angles of 13.59° and 21.44° were found. On the other hand, thiophene methylation decreases the thiophene-acridine angle from 85.67° in **1c** to 77.42° in **1d**. The measured dihedral angles and the optimized geometries are shown in Figure 4. Figure 4 also illustrates that the orthogonality of the peripheral donor groups over two torsion angles to the TTT core is not uniform between the three symmetrically equivalent donor positions (with some rather coplanar, others quite orthogonal) indicating that the configuration at any given instant differs significantly from a time-averaged configuration, in which the peripheral donors occupy a more globular space.

The characteristics of the excited states were investigated using TD-DFT and SOC-TD-DFT. For **1a** and **1b** the first absorption band (Figure S7) observed experimentally is related to the three low-lying states. Interestingly, the S_1, S_2, and S_3 states of these two carbazole derivatives have CT orbital configurations that stretch both over the carbazole and part of the TTT-thiophene core. Still, the oscillator strengths *f* for these transitions are relatively high, characteristic of a LE state. Therefore, for both compounds, the excited state is attributed as a mixed ^{1}LE/^{1}CT state, with **1b** having the larger LE character due to the larger value of *f*. S_1 is associated with the one of the three thiophene-carbazole arms where the largest thiophene-carbazole dihedral angle is observed. S_2 and S_3 are similar states but involve the other arms of the molecule with lower dihedral angles due to configurational asymmetry. For **1c** and **1d** the first absorption band is related to the three low-lying CT states

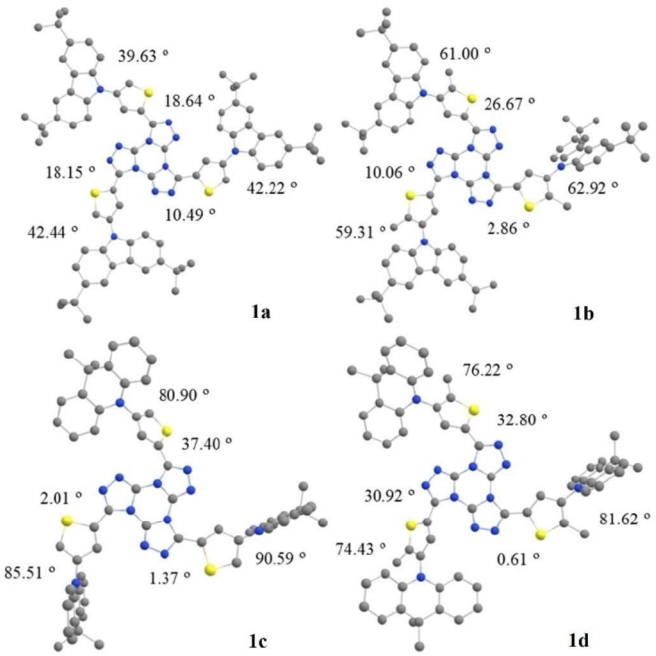

Figure 4. Optimized ground state geometries within B3LYP/def2-SVP level of theory.

from acridine to the TTT-thiophene core as indicated by the low values of *f* and the orbital configuration. The second band in the theoretical spectra for all compounds, which corresponds to the high energy band observed experimentally, is related to the LE states from the TTT-thiophene core. Detailed information about these excited states is given in Tables S1–S4.

The optimized S_1 and T_1 geometries were obtained to gain information on the S_1 and triplet states. In the optimized S_1 state geometry, only minor differences between the dihedral angles are observed (Figure S8), leading to only slight changes of *f* for the $S_0 \rightarrow S_1$ transition in all compounds (Table S1-S4). On the other hand, from the ground state to T_1, the geometry of the molecules flattens significantly, decreasing the dihedral angles between the donor and acceptor moieties (Figure S9). The configuration of the excited triplet states was calculated using SOC-TD-DFT starting from the T_1 state geometry. The flattening of the structure increases the overall conjugation of the π-system leading to low-lying states with a LE orbital configuration (Table S1–S4). Therefore, the T_1, T_2, and T_3 states are assigned as ^{3}LE from the TTT-thiophene core, the lowest energy state being the one with the smallest dihedral angle between these two moieties. The T_4 state is energetically close to S_1 and has a CT orbital configuration from donor to acceptor moieties.

The SOC effects on the ISC and phosphorescence pathways were evaluated using the SOC matrix elements (SOCME) obtained from SOC-TD-DFT calculations (Table 3). The ISC rate is proportional to the sum of the SOCME between S_1 and all triplet states of lower or similar energy (in this case, T_1-T_4 for all compounds). For **1a** and **1b** the SOCME sum between S_1 and the triplet states is 4.36 and 5.19 cm^{-1}, while for **1c** and **1d** we

Table 3. SOCME and adiabatic energy differences.

	1a	1b	1c	1d
$\sum_j \left(\langle T_{j=1-4\,(x,y,z)}\lvert\hat{H}_{SOC}\rvert S_1\rangle\right)^2$ [cm^{-1}]	4.36	5.19	3.75	1.75
$\sum_i \left(\langle T_{1(x,y,z)}\lvert\hat{H}_{SOC}\rvert S_{i=1-10}\rangle\right)^2$ [cm^{-1}]	10.36	9.37	11.65	14.54
S_1 [eV]	3.231	3.346	2.972	3.112
T_1 [eV]	2.207	2.256	2.061	2.245
ΔE_{ST} [eV]	1.024	1.090	0.911	0.867

found 3.75 and 1.75 cm^{-1}. These values agree with the measured quantum yields Φ. **1a** and **1d** have larger Φ than their homologs, which is mainly due to the fluorescence emission indicating less deactivation through the ISC pathway. Such values of SOCME for the ISC pathway are similar to those of regular donor-acceptor molecules and sulfur containing compounds.[12]

The SOCME between all the low-lying states allows the a priori forbidden $T_1 \rightarrow S_0$ radiative pathway. We calculated the SOCME between T_1 and the first ten excited singlet states. For **1a** and **1b**, this sum of SOCME is 10.36 and 9.37 cm^{-1}. As the T_1 energies of these two compounds are very similar, the SOCME sums found agree with the experimental observation of a lower k_{Phosph} and thus a higher τ_{Phosph} with **1b**. For **1c** and **1d** the sum of SOCME is 11.65 and 14.54 cm^{-1}. Here, **1d** has a larger SOCME between the low-lying states and a higher T_1 energy than **1c**. As k_{Phosph} is proportional both to the SOCME and to the T_1 energy, **1d** accordingly shows a significantly lower τ_{Phosph} compared to the other three compounds and only very weak RTP. The phosphorescence pathway shows relatively larger values of SOCME and is comparable to other molecules with RTP.[13] As the low-lying triplet states are ^{3}LE states centered both at the TTT core and the thiophene bridge, the thiophene inclusion increases the SOC associated with the radiative $T_1 \rightarrow S_0$ pathway, thus allowing RTP.

Conclusion

In summary, including thiophene bridges between the donor and acceptor moieties in D_3A-type tristriazolotriazines resulted in an RTP emission in solution with a lifetime of 0.1–3.5 ms. Furthermore, all compounds exhibited PF emission with a PLQY between 0.023 and 0.258, with carbazole derivatives showing higher efficiency. The PF originates from a mixed ^{1}LE/^{1}CT state in the carbazole homologs, while the acridine variants showed pure ^{1}CT emission due to the good orthogonality between the donor and acceptor moieties. For compounds **1a**, **1b**, and **1c** with longer phosphorescence lifetime, a concurrent TTA mechanism is observed. The comparison between solution and solid-state emission and their lifetimes suggests that the bulky donor moieties protect the emissive ^{3}LE state which spreads through the TTT-thiophene core. The partially protected localization of the emissive triplet state at the molecular core, which is surrounded by three bulky donor units, likely assists the strong SOC between the low-lying states of about 10 cm^{-1} in allowing RTP to manifest itself even in solution. We conclude that the incorporation of thiophene bridges in D_nA-type emitters should be considered in molecular design aiming at solution RTP.

Acknowledgements

We are grateful to CAPES (Coordenação de aperfeiçoamento de pessoal de nível superior, Brazil, finance code #937-20 and #001) and COFECUB (Comité français d'évaluation de la coopération universitaire et scientifique avec le Brésil) (joint project Ph-C 962/20), FAPESC, INCT-INEO and H2020-MSCA-RISE-2017 (OCTA, #778158) for support. H.M.L. is grateful to the French ministry for Foreign Affairs for an Eiffel scholarship. S.K. and A.P.M. acknowledge funding from the EPSRC grant EP/T02240X/1. We thank Piere Dechambenoit for help with cyclic voltammetry, and Emmanuelle Hamon for the TGA analyses.

Conflict of Interest

The authors declare no conflict of interest.

Data Availability Statement

The data that support the findings of this study are available from the corresponding author upon reasonable request.

Keywords: delayed fluorescence · heavy atom effect · phosphorescence · room temperature tristriazolotriazine

[1] a) S. Hirata, *Adv. Opt. Mater.* **2017**, *5*, 1700116; b) N. Gan, H. Shi, Z. An, W. Huang, *Adv. Funct. Mater.* **2018**, *28*, 1802657; c) S. R. Forrest, M. A. Baldo, D. F. O'Brien, Y. You, A. Shoustikov, S. Sibley, M. E. Thompson, *Nature* **1998**, *395*, 151; d) X. Zhen, Y. Tao, Z. An, P. Chen, C. Xu, R. Chen, W. Huang, K. Pu, *Adv. Mater.* **2017**, *29*, 1606665.

[2] R. C. Evans, P. Douglas, C. J. Winscom, *Coord. Chem. Rev.* **2006**, *250*, 2093–2126.

[3] a) M. A. El-Sayed, *J. Chem. Phys.* **1963**, *38*, 2834; b) N. J. Turro, *Modern Molecular Photochemistry*, University Science Books, Sausalito, **1991**, pp. 99–100.

[4] T. Zhang, X. Ma, H. Wu, L. Zhu, Y. Zhao, H. Tian, *Angew. Chem. Int. Ed.* **2020**, *59*, 11206–11216; *Angew. Chem.* **2020**, *132*, 11302–11312.

[5] a) X.-K. Ma, Y. Liu, *Acc. Chem. Res.* **2021**, *54*, 3403–3414; b) S. Kuila, K. V. Rao, S. Garain, P. K. Samanta, S. Das, S. K. Pati, M. Eswaramoorthy, S. J. George, *Angew. Chem. Int. Ed.* **2018**, *57*, 17115–17119; *Angew. Chem.* **2018**, *130*, 17361–17365; c) W.-L. Zhou, Y. Chen, Q. Yu, H. Zhang, Z.-X. Liu, X.-Y. Dai, J.-J. Li, Y. Liu, *Nat. Commun.* **2020**,*11*, 4655; d) J. Xu, A. Takai, Y. Kobayashi, M. Takeuchi, *Chem. Commun.* **2013**, *49*, 8447; e) B. Ventura, A. Bertocco, D. Braga, L. Catalano, S. d'Agostino, F. Grepioni, P. Taddei, *J. Phys. Chem. C* **2014**, *118*, 18646; f) G. D. Gutierrez, G. T. Sazama, T. Wu, M. A. Baldo, T. M. Swager, *J. Org. Chem.* **2016**, *81*, 4789.

[6] M. K. Etherington, J. Gibson, H. F. Higginbotham, T. J. Penfold, A. P. Monkman, *Nat. Commun.* **2016**, *7*, 13680.

[7] a) S. Zeng, C. Xiao, J. Zhou, Q. Dong, Q. Li, J. Lim, H. Ma, J. Y. Lee, W. Zhu, Y. Wang, *Adv. Funct. Mater.* **2022**, *32*, 2113183; b) Z. Fang, S. Wang, J. Liao, X. Chen, Y. Zhu, W. Zhu, Y. Wang, Yafei, *J. Mater. Chem. C* **2022**, *10*, 4837–4844; c) R. Hojo, D. M. Mayder, Z. M. Hudson, *J. Mater. Chem. C* **2022**, *10*, 13871–13877; d) X. Chen, S. Wang, H. L. Lee, J. Y. Lee, X. Liao, L. Li, W. Zhu, Y. Wang, *Adv. Opt. Mater.* **2021**, *9*, 2101518; e) S. Wang, X. Wang, K. H. Lee, S. Liu, J. Y. Lee, W. Zhu, Y. Wang, *Dyes Pigm.* **2020**, *182*, 108589; f) S. K. Pathak, Y. Xiang, M. Huang, T. Huang, X. Cao, H. Liu, G. Xie, C. Yang, *RSC Adv.* **2020**, *10*, 15523–15529; g) F. Hundemer, E.

Crovini, Y. Wada, H. Kaji, S. Bräse, E. Zysman-Colman, *Mater Adv* **2020**, *1*, 2862–2871.

[8] a) C. Feng, S. Li, L. Fu, X. Xiao, Z. Xu, Q. Liao, Y. Wu, J. Yao, H. Fu, *J. Phys. Chem. Lett.* **2020**, *11*, 8246–8251; b) M. Li, W. Xie, X. Cai, X. Peng, K. Liu, Q. Gu, J. Zhou, W. Qiu, Z. Chen, Y. Gan, S. J. Su, *Angew. Chem. Int. Ed.* **2022**, *61*, e202209343; c) I. S. Park, H. Min, T. Yasuda, *Angew. Chem. Int. Ed.* **2022**, *61*, e202205684; d) S. M. Pratik, V. Coropceanu, J.-L. Bredas, *ACS Materials Lett.* **2022**, *43*, 440–447; e) I. S. Park, M. Yang, H. Shibata, N. Amanokura, T Yasuda, *Adv. Mater.* **2022**, *34*, 2107951; f) T. Hua, L. Zhan, N. Li, Z. Huang, X. Cao, Z. Xiao, S. Gong, C. Zhou, C. Zhong, C. Yang, *Chem. Eng. J.* **2021**, *426*, 131169.

[9] T. Matulaitis, P. Imbrasas, N. A. Kukhta, P. Baronas, T. Buciunas, D. Banevicius, K. Kazlauskas, J. V. Grazulevicius, S. Jursenas, *J. Phys. Chem. C* **2017**, *121*, 23618–23625.

[10] R. Dhali, D. K. A. P. Huu, F. Bertocchi, C. Sissa, F. Terenziani, A. Painelli, *Phys. Chem. Chem. Phys.* **2021**, *23*, 378–387.

[11] a) A. Navarro, M. P. Fernández-Liencres, G. García, J. M. Granadino-Roldán, M. Fernández-Gómez, *Phys. Chem. Chem. Phys.* **2014**, *17*, 605–618; b) R. Cristiano, H. Gallardo, A. J. Bortoluzzi, I. H. Bechtold, C. E. M. Campos, R. L. Longo, *Chem. Commun.* **2008**, 5134–5136; c) T. Yasuda, T. Shimizu, F. Liu, G. Ungar, T. Kato, *J. Am. Chem. Soc.* **2011**, *133*, 13437–13444.

[12] a) J. Gibson, A. P. Monkman, T. J. Penfold, *ChemPhysChem* **2016**, *17*, 2956–2961; b) A. Lv, W. Ye, X. Jiang, N. Gan, H. Shi, W. Yao, H. Ma, Z. An, W. Huang, *J. Phys. Chem. Lett.* **2019**, *10*, 1037–1042.

[13] a) C. A. M. Salla, G. Farias, M. Rouzières, P. Dechambenoit, F. Durola, H. Bock, B. de Souza, I. H. Bechtold, *Angew. Chem. Int. Ed.* **2019**, *58*, 6982–6986; *Angew. Chem.* **2019**, *131*, 7056–7060; b) G. Farias, C. A. M. Salla, M. Aydemir, L. Sturm, P. Dechambenoit, F. Durola, B. de Souza, H. Bock, A. P. Monkman, I. H. Bechtold, *Chem. Sci.* **2021**, *12*, 15116–15127.